Combust. Theory Modelling 4 (2000) 241–264. Printed in the UK PII: S1364-7830(00)11439-1

Comparison of a spectral model for premixed turbulent flame propagation to DNS and experiments

Mark Ulitsky†, Chaouki Ghenaï‡, Iskender Gökalp§, Lian-Ping Wang‖ and Lance R Collins¶

† MS B216, T-3, Los Alamos National Laboratory, Los Alamos, NM 87545, USA
‡ Mechanical and Aerospace Engineering Department, UCLA, Los Angeles, CA 90095-1597, USA
§ LCSR-CNRS, 1c Av. de la Recherche Scientifique, Orléans, 45071, France
‖ Department of Mechanical Engineering, University of Delaware, Newark, DE 19716, USA
¶ Department of Chemical Engineering, Penn State University, University Park, PA 16802, USA

E-mail: LXC12@psu.edu (Lance R Collins)

Received 31 January 2000, in final form 4 July 2000

Abstract. A recently developed spectral model for premixed turbulent combustion in the flamelet regime (based on the EDQNM turbulence theory) has been compared with both direct numerical simulations (DNS) and experimental data. The 128^3 DNS is performed at a Reynolds number of 223 based on the integral length scale. Good agreement is observed for both single- and two-point quantities (i.e. ratio of the turbulent to laminar burning velocities, scalar autocorrelation, dissipation and scalar-velocity cross correlation spectra) for the two different values of u'/s_{L0} considered. The model also predicts the rapid transient behaviour of the flame at early times. An experimental set-up is then described for generating a lean methane–air flame and measuring two-point spatial correlations along the midpoint of the flame brush (i.e. along the $\overline{C} = 0.5$ contour). The experimental measurements in the flamelet regime take the form of a discontinuous or 'telegraph' signal. The EDQNM model, in contrast, describes an 'ensemble' of flames, and thus is based solely on continuous variables. A theoretical relationship between the correlation obtained from the EDQNM model and the equivalent correlation for a discontinuous (experimental) flame is derived. The relationship is used to enable a meaningful comparison between experimentally observed and model correlations. In general, the agreement is good for the three different cases considered in this study, with most of the error occurring at the lowest Reynolds number ($Re_L = 22$). Furthermore, it is shown that considerably more error would result if no attempt is made to convert the ensemble representation in the model to an equivalent single-flame or 'telegraph' signal.

1. Introduction

The interaction between fully developed turbulence in the unburnt reactants and a propagating flame remains one of the open questions in combustion modelling. If we restrict our attention to the case of flames that are thin compared with all of the length scales associated with the turbulent fluctuations, then turbulence primarily stretches the flame surface without affecting the chemical reactions within the flame very much. This regime, first identified by Damköhler (1940), is often referred to as flamelet combustion. Flamelet combustion is important from a technological viewpoint since many combustion devices (e.g. internal combustion engines, gas turbines) operate in this regime. Despite the enormous simplification implied by flamelet combustion, there is still no comprehensive theory to describe turbulent flame propagation at this time.

1364-7830/00/030241+24$30.00

Part of the difficulty is related to the topologically complex nature of a flame surface that is wrinkled by turbulence. Direct numerical simulations (DNS) and experimental measurements (Dandekar and Collins 1995, Mantzaras *et al* 1989, North and Santavicca 1990) both indicate that a flame surface exposed to fully developed turbulence will contain large-, intermediate- and small-scale wrinkles randomly distributed throughout. Moreover, earlier results in our group (Collins 1995b) demonstrated that the contribution from intermediate to fine-scale wrinkling can be significant (even dominant) in terms of the total surface area that is produced. This implies that the entire energy spectrum is active in the process of wrinkling the flame, suggesting that a reasonable flamelet model must, from the outset, account for contributions to the surface area from the entire energy spectrum.

This fact was recognized over ten years ago independently by Gouldin (1987), Kerstein (1988) and Peters (1988) who attempted to account for the broad range of scales by assuming a fractal dimension for the flame surface. By definition, a fractal surface contains wrinkles that are self-similar with respect to the size of the wrinkles. For such a surface, a single scaling parameter (the fractal dimension) can relate the surface area to the cross sectional area. Experimental measurements (North and Santavicca 1990) and numerical simulations (Collins 1995a) have shown that flames are fractal-like over at least a range of scales, but a serious deficiency with this approach is that the fractal dimension is not a constant, but instead is a function of flamelet parameters such as the ratio of the turbulence intensity to the laminar flame speed. Accounting for this functionality adds several *ad hoc* corrections to the model. Moreover, a fractal model is only appropriate for turbulence that is fully developed and for flames that have had sufficient time to develop the characteristic self-similar wrinkles. Thus, time-dependent flows (e.g. those encountered in internal combustion engines) may not be well represented by a fractal flamelet model.

The renormalized group theory (RNG) has been applied to premixed flame propagation by Yakhot (1988) and Sivashinsky (1988). The goal of these theories is to account for successive scales of wrinkling by renormalizing the system parameters (usually the flame speed). In principle, this approach accounts for all of the scales of wrinkling; however, as noted in a recent study by Denet (1998), renormalization of just the turbulent flame speed may not account for non-local interactions between small-scale turbulence and large-scale wrinkles on the flame surface. This aspect of premixed flames appears to be connected to the fundamentally nonlinear nature of propagation itself, and must therefore be accounted for in a self-consistent flamelet theory.

In recent papers (Collins and Ulitsky 1996, Ulitsky and Collins 1997a), our group has proposed an alternative modelling strategy that addresses some of the weaknesses of the fractal and RNG models. In this model, the flame surface is represented by a scalar spectrum that arises from taking the Fourier transform of two-point statistics in the flame. Two-point statistics provides a natural means of introducing the energy spectrum (and hence the broad distribution of scales) into the analysis. Our approach is similar to that taken by Peters (1992), although the models differ significantly in their details. Whereas Peters (1992) applies a local closure for the propagation term, closure of both the convective and propagation terms in our model involve convolution integrals, and so non-local interactions, such as those described by Denet (1998), are completely accounted for. Furthermore, the spectrum is evolved in time, so there is no implicit assumption of self-similarity required by the theory. Of course, the spectrum may evolve into a self-similar form over time (Collins 1995b), but that too is captured by this approach.

The model is based on the Kuramoto–Sivashinsky equation for a propagating flame surface (Sivashinsky 1977), modified for three-dimensional turbulence by Dandekar and Collins (1995). This equation describes a flame surface (or more precisely an ensemble of flame

surfaces) that propagates into the reactants with the laminar flame velocity, is advected by the local fluid velocity, and is subject to hydrodynamic and thermal–diffusive instabilities. Hydrodynamic and thermal–diffusive instabilities are modelled by introducing disturbance growth factors taken from the linear stability analysis of a flame (Sivashinsky 1977, 1979, 1983). Turbulence is introduced into the assumed incompressible velocity field through the initial conditions. The flame surface shape is then updated by solving a conservation equation for a scalar field variable $G(\boldsymbol{x}, t)$ defined such that its isocontours are flame surfaces (see Dandekar and Collins 1995 for a complete description of the equation). The ensemble of flame surfaces corresponds to the ensemble of isocontours of the field variable $G(\boldsymbol{x}, t)$. From its definition and simple geometric considerations, it is relatively straightforward to determine flame surface statistics and the turbulent burning velocity from $G(\boldsymbol{x}, t)$.

Ulitsky and Collins (1997a) derived transport equations for two-point statistics of the scalar $G(\boldsymbol{x}, t)$ and the local fluid velocity, $\boldsymbol{u}(\boldsymbol{x}, t)$ and Fourier transformed them to obtain a spectral description of the scalar field. Then, by applying the eddy-damped quasi-normal Markovian (EDQNM) approximation (Lesieur 1987, Orszag 1970), they obtained a closed set of integro-differential equations that describe the evolution of the scalar spectrum. Previously, EDQNM had been successfully applied to isotropic turbulence (Leith 1971, Herring 1974, Andre and Lesieur 1977, Lesieur *et al* 1987), anisotropic turbulence (Cambon *et al* 1981, Nakauchi 1984), and passive scalars (Herring *et al* 1982, Herr *et al* 1996), providing confidence that the same closure strategy would be effective for modelling a propagating scalar as well. Several properties of the flame surface, including the average turbulent burning velocity, can be obtained from simple integrals of the scalar spectrum.

There are two uncertainties in the proposed spectral model that this paper addresses. First, we must determine how well the EDQNM closure approximation describes the higher-order moments of the spectral transport equations. An earlier study of a passive scalar (Herr *et al* 1996) showed good agreement between a similar EDQNM model and direct numerical simulations. However, the present model contains a number of new complexities that have yet to be evaluated, and hence a comparison with numerical simulations is appropriate. Second, even if the EDQNM model is effective at representing the Kuramoto–Sivashinsky equation, there remains the question of how well this equation describes real premixed flames. We address this issue by comparing the EDQNM model with two-point experimental measurements. In order to accomplish this, a relationship was derived between the EDQNM model, which describes an ensemble of flames, and the experiment, which contains only a single flame at any given instant. This non-trivial relationship enables us to directly compare the experimental measurements with theory.

The paper is arranged as follows. A brief summary of the governing equations is given in section 2 (the interested reader should refer to Ulitsky and Collins (1997a) for more details). This is followed by a comparison of the modelling results with DNS in section 3. Section 4 describes the experimental apparatus and section 5 shows the extension of the EDQNM model to an experimental flame. The comparison between experiment and theory is then given in section 6 followed by conclusions in section 7.

2. Governing equations

Several previous studies of turbulent flame propagation employed a field equation to describe the evolution of the thin flame sheet (Kerstein *et al* 1988, Ashurst *et al* 1988, Yakhot 1988, Osher and Sethian 1988, Ashurst and Sivashinsky 1991, Aldredge 1992, Zhu and Ronney 1994, Collins 1995b, Ulitsky and Collins 1997b). They focused primarily on the Huygen equation

which takes the form

$$\frac{\partial G}{\partial t} + \frac{\partial}{\partial x_i}(u_i G) = s_L \sqrt{\frac{\partial G}{\partial x_i}\frac{\partial G}{\partial x_i}} \tag{1}$$

where flame surfaces are identified by isocontours of $G(x, t)$ and s_L represents the local laminar flame speed, which, in general, is a function of both the local flame curvature and flow strain (Huang *et al* 1998, Clavin and Joulin 1997, Joulin 1994). The field variable $G(x, t)$ represents an ensemble of flame surfaces, which can be distinguished by introducing a mean gradient in the direction of nominal flame propagation (the x_3-direction has been arbitrarily chosen in this study). In order to accommodate most pseudospectral formulations of this problem, a linear transformation involving G is necessary, as G is not periodic in the direction of flame propagation once the mean gradient has been imposed. This transformation can be simply expressed as (Kerstein *et al* 1988)

$$g(x, t) = G(x, t) - x_3 \tag{2}$$

where $g(x, t)$, by definition, is periodic in all three directions.

Although ideally we would like to apply the EDQNM turbulence theory to the Huygen equation, its nonlinear representation of propagation is not readily amenable to analysis. It is far more practical and mathematically more tractable to use a different nonlinear representation first proposed by Sivashinsky (1977), and then developed by Dandekar and Collins (1995) in a numerical study of turbulent premixed flames. Furthermore, we neglect hydrodynamic and thermo-diffusive instabilities in this formulation, even though they are linear. The reason is that the EDQNM modelling of these terms, which are dominant at small wavenumbers, leads to an expression that grows exponentially fast with time. The problem arises from the Markovian approximation of the time evolution of the triple correlations, which yields an unphysical result when there is unstable forcing. In principle, a more general treatment of the triple correlations would eliminate this problem; however, this is beyond the scope of the present study. To eliminate these terms, we make the additional assumptions of unity Lewis number and negligible heat release to arrive at the governing equation

$$\frac{\partial g}{\partial t} + \frac{\partial}{\partial x_i}(u_i g) + u_3 = s_{L0}\left(1 + \frac{1}{2}\frac{\partial g}{\partial x_i}\frac{\partial g}{\partial x_i} + \frac{\partial g}{\partial x_3}\right) + s_{L0}L_M\frac{\partial^2 g}{\partial x_i \partial x_i} \tag{3}$$

where s_{L0} is the laminar flame speed of an unstretched flame, and L_M, the Markstein length, is a parameter that scales with the laminar flame thickness. Although the presence of the $\frac{\partial g}{\partial x_3}$ term on the right-hand side of equation (3) seems rather benign at this stage, it greatly complicates the EDQNM analysis during the Markovianization step. Numerical simulations with and without this term have shown that its contribution to the turbulent flame speed is relatively small. Consequently, this term has been neglected, and the actual scalar equation to be used for simulation and modelling purposes is

$$\frac{\partial g}{\partial t} + \frac{\partial}{\partial x_i}(u_i g) + u_3 = s_{L0}\left(1 + \frac{1}{2}\frac{\partial g}{\partial x_i}\frac{\partial g}{\partial x_i}\right) + s_{L0}L_M\frac{\partial^2 g}{\partial x_i \partial x_i}. \tag{4}$$

The thin flame sheet is propagating through three-dimensional, forced, isotropic turbulence that is described by the incompressible Navier–Stokes and continuity equations. A solenoidal random forcing function is used to achieve and maintain stationary turbulence (Eswaran and Pope 1988).

The objective of the EDQNM theory is to predict the evolution of the turbulent energy and scalar spectra. The present study uses the model developed by Ulitsky and Collins (1997a). Here we present a brief summary of the governing equations in skeleton form; the interested reader should refer to the earlier manuscript for a detailed description of the model. In this theory, the evolution of the flame surface is represented by three correlations

$$\begin{aligned} B(r) &= \overline{g'(x)g'(x+r)} \\ Q_i(r) &= \overline{u_i'(x)g'(x+r)} \\ R_{ij}(r) &= \overline{u_i'(x)u_j'(x+r)} \end{aligned} \tag{5}$$

where $'$ refers to the fluctuating component. Spectral statistics are obtained by taking the Fourier transform of the correlations, yielding for example

$$B(\boldsymbol{k}) = \int B(\boldsymbol{r})\, \mathrm{e}^{-\mathrm{i}\boldsymbol{k}\cdot\boldsymbol{r}}\, \mathrm{d}\boldsymbol{r}. \tag{6}$$

Similar integrals define $Q_i(\boldsymbol{k})$ and $R_{ij}(\boldsymbol{k})$. If we assume the turbulent kinetic energy to be isotropic and helicity free, we can simplify the functional dependence of the spectra as shown below

$$\begin{aligned} B(\boldsymbol{k}) &= 2B(k,\mu) \\ Q_i(\boldsymbol{k}) &= Q(k,\mu)P_{i3}(\boldsymbol{k}) \\ R_{ij}(\boldsymbol{k}) &= R(k)P_{ij}(\boldsymbol{k}) \end{aligned} \tag{7}$$

where

$$\begin{aligned} P_{ij}(\boldsymbol{k}) &\equiv \delta_{ij} - \frac{k_i k_j}{k^2} \\ k &\equiv |\boldsymbol{k}| \\ \mu &\equiv \frac{k_3}{k} \end{aligned} \tag{8}$$

and δ_{ij} is the Kronecker delta function. As a consequence of equation (7), the Reynolds stress tensor is defined entirely by a single scalar spectrum, $R(k)$ (note, most publications refer to the energy spectrum $E(k)$ which is defined as $R(k)k^2/(2\pi^2)$). In contrast, correlations involving the scalar are *axisymmetric* with respect to the direction of nominal flame propagation. This introduces a dependence of the spectrum on μ, which is the cosine of the angle between the wavevector $\boldsymbol{k}$ and the direction of nominal flame propagation (here taken to be x_3). Note that the relationships shown in equation (7) are based solely on the spatial symmetries of the problem, and as such may be considered exact.

Despite this great simplification, it is still difficult to evaluate numerically the k and μ dependence of the scalar spectra. Herring (1974) suggested an alternative approach. The implicit dependence on the angle μ can be made explicit by introducing a Legendre polynomial series expansion for each scalar spectrum, as shown below

$$\begin{aligned} B(k,\mu) &= \sum_{n=0}^{\infty} B_{2n}(k)L_{2n}(\mu) \\ Q(k,\mu) &= \sum_{n=0}^{\infty} Q_{2n}(k)L_{2n}(\mu) \end{aligned} \tag{9}$$

where $L_{2n}(\mu)$ is the Legendre polynomial of order $2n$, and $B_{2n}(k)$ and $Q_{2n}(k)$ are the spectral coefficients for each order. Only even-ordered powers of the Legendre polynomials appear in

equation (9) because $B(k, \mu)$ and $Q(k, \mu)$ can be shown to be even functions of μ (Ulitsky and Collins 1997a). Note that the zeroth-order terms provide the isotropic contribution to the infinite series, while the higher-order terms account for the anisotropy that is introduced into the scalar field as a result of the presence of the uniform mean gradient. For practical purposes, the above infinite sums are truncated beyond $n = 2$. (Note that Ulitsky and Collins (1997a) showed that the terms corresponding to $n = 2$ are much smaller than the lower-order terms, and so contributions from the neglected higher-order terms are expected to be negligible.) The model has six scalar correlations to evaluate ($B_0(k)$, $B_2(k)$, $B_4(k)$, $Q_0(k)$, $Q_2(k)$ and $Q_4(k)$). Here, we summarize the final equations for the six scalar spectra in skeleton form (see Ulitsky and Collins 1997a for details)

$$\begin{aligned}\left[\frac{\partial}{\partial t} + 2s_{L0}L_M k^2\right] B_{2n}(k) &= S^B_{2n}(k) + T^B_{2n}(k) + P^B_{2n}(k)\\ \left[\frac{\partial}{\partial t} + (s_{L0}L_M + \nu)k^2\right] Q_{2n}(k) &= S^Q_{2n}(k) + T^Q_{2n}(k) + P^Q_{2n}(k).\end{aligned} \tag{10}$$

$S^B_{2n}(k)$ and $S^Q_{2n}(k)$ are the linear source terms which are exact and take the form

$$\begin{aligned}S^Q_0(k) &= -R(k)\\ S^Q_2(k) &= S^Q_4(k) = 0\\ S^B_0(k) &= -\tfrac{2}{3}Q_0(k) + \tfrac{2}{15}Q_2(k)\\ S^B_2(k) &= \tfrac{2}{3}Q_0(k) - \tfrac{10}{21}Q_2(k) + \tfrac{4}{21}Q_4(k)\\ S^B_2(k) &= \tfrac{12}{35}Q_2(k) - \tfrac{38}{77}Q_4(k).\end{aligned} \tag{11}$$

The remaining functions arise from *nonlinearities* due to advection ($T^B_{2n}(k)$ and $T^Q_{2n}(k)$) and propagation ($P^B_{2n}(k)$ and $P^Q_{2n}(k)$). Nonlinear terms give rise to higher-order moments that require a closure approximation. Here, the EDQNM formalism is used to obtain approximate expressions that take the form of convolution integrals. At each time step, the convolution integrals are evaluated using the numerical method described in Herr *et al* (1996).

The traditional scalar–scalar and scalar–velocity spectra can be expressed as follows:

$$E_g(k) \equiv \frac{k^2}{\pi^2}B_0(k) \tag{12}$$

$$E_{u_3 g}(k) \equiv \frac{k^2}{3\pi^2}\left[Q_0(k) - \frac{Q_2(k)}{5}\right] \tag{13}$$

where by definition

$$\begin{aligned}\overline{g'^2} &= \int_0^{k_{\max}} E_g(k)\,\mathrm{d}k\\ \overline{u'_3 g'} &= \int_0^{k_{\max}} E_{u_3 g}(k)\,\mathrm{d}k.\end{aligned} \tag{14}$$

Furthermore, the ratio of the turbulent to laminar flame speed (s_T/s_{L0}) can be calculated from the scalar dissipation spectrum

$$\frac{s_T}{s_{L0}} \equiv \frac{1}{s_{L0}}\frac{\mathrm{d}\overline{g}}{\mathrm{d}t} = 1 + \tfrac{1}{2}\overline{\nabla g \cdot \nabla g} = 1 + \tfrac{1}{2}\overline{\nabla g' \cdot \nabla g'} = 1 + \tfrac{1}{2}\int_0^{k_{\max}} k^2 E_g(k)\,\mathrm{d}k \tag{15}$$

where the advective and diffusive terms fall out from homogeneity and linearity, respectively, and we have used the fact that there are no mean gradients in the g-field (recall that the uniform

mean gradient is imposed upon the G-field). We will use these relationships to compare our results with the numerical simulations and experiments.

In addition to the governing equations, it is important to identify the controlling parameters in the problem. For the fluid, since we assume homogeneous isotropic turbulence, the velocity is completely parametrized by the turbulent intensity u', the dissipation rate of kinetic energy ϵ and the fluid viscosity ν (or alternatively the Kolmogorov length scale, $\eta \equiv (\nu^3/\epsilon)^{1/4}$). The flame equations explicitly introduce two other parameters, the laminar flame velocity, s_{L0}, and the Markstein length, L_M. There are other implicit parameters as well. For example, the flame speed may depend on the temperature ratio of the products to unburnt reactants, β, the Lewis number of the limiting reactant in the flame, Le, and the flame thickness, d.

The three fluid parameters can be consolidated into a single dimensionless parameter, the Reynolds number. In effect, by specifying the Reynolds number you define the ratio of the largest to smallest turbulence scales. The laminar flame velocity is normally made dimensionless by the turbulence intensity, i.e. u'/s_{L0}. The Markstein length is then usually given in terms of a Markstein number (here defined as $Ma \equiv L_M/d$, which can be a function of β, Le and the Prandtl and Zeldovich numbers), and the flame thickness, d, is then obtained either by direct experimental observation or by assuming a constitutive relationship of the form (Glassman 1987)

$$d = C_d \frac{\nu}{s_{L0}}. \tag{16}$$

We note that there is some uncertainty as to the value of the dimensionless coefficient C_d shown in equation (16). Scaling arguments suggest a value of the order of unity (Clavin and Williams 1982), whereas experimental measurements have yielded values as large as 10 (Lee *et al* 1993). As noted in two earlier publications (Collins and Ulitsky 1996, Ulitsky and Collins 1997a) the results are *very sensitive* to the flame thickness. We therefore use experimental observations of the flame thickness in the present study to eliminate this uncertainty.

The present study (both the comparison with DNS and experiment) will focus on the parametric dependence of the flames on what is generally considered the most important parameter, namely the non-dimensional turbulence intensity u'/s_{L0}. Earlier work (Dandekar and Collins 1995) has shown that effects due to other parameters such as Lewis number can be incorporated into the present spectral modelling framework; however, this requires a generalization of the Markovianization step of the EDQNM procedure.

3. Direct numerical simulations

We can assess how accurately the EDQNM theory captures the nonlinear dynamics of the proposed field equation by comparing the predictions to DNS data. In particular, we will focus on making steady-state comparisons of the scalar autocorrelation and dissipation spectra, as well as the scalar-velocity cross correlation spectrum for two different values of u'/s_{L0} ($u'/s_{L0} = 1$ and 3). The dissipation spectrum is especially relevant, since the ratio of the turbulent to laminar flame speed is obtained from an integral of this spectrum. We shall also investigate the transient behaviour of the turbulent flame speed to test how well the model predicts the rapid equilibration of the flame with the turbulence. The discussion of the DNS set-up is presented below.

Direct numerical simulations of the continuity, Navier–Stokes and modified Sivashinsky equations are performed on a 128^3 uniform grid using a standard pseudospectral Galerkin

method to update the velocity field and location of the flame front (Wang *et al* 1996, 1999, Canuto *et al* 1988). In essence, the algorithm is identical to that used in Herr *et al* (1996) for updating a passive scalar in isotropic turbulence, with the only change now arising from the dissipative nonlinearity introduced into the field equation by propagation (see equation (4)). The linear terms in the governing equations (in Fourier space) are solved for exactly using an integrating factor technique, and a second-order Adams–Bashforth scheme is employed for the time integration. Aliasing errors resulting from the pseudospectral calculation of the nonlinear terms are removed via the two-thirds rule, which effectively truncates all modes greater than $2k_{\max}/3$. To ensure adequate spatial resolution of the small length scales, the fluid viscosity is chosen such that the criterion suggested by Eswaran and Pope (1988) (i.e. $k_{\max}\eta > 1$) is satisfied. In this study, $k_{\max}\eta$ has a value of 1.56, and the CFL number, which is a commonly used measure of temporal resolution, is 0.23. The velocity field is made stationary by maintaining constant total energy in each of the first two wavenumber shells ($0.5 \leqslant k \leqslant 1.5$ and $1.5 \leqslant k \leqslant 2.5$), with the energy ratio between the two shells consistent with $k^{-5/3}$. Since the nodes are not evenly distributed in the spherical shells in wavevector space, a smoothing operation (Eswaran and Pope 1988) is applied to the energy spectrum $E(k)$.

To achieve stationarity in the flow field, the direct numerical simulation of the turbulence is run for about 10 eddy turnover times. The scalar field representing the flame front is then introduced, and the velocity field and flame front are jointly evolved for 60 eddy turnover times. The scalar field, which is initialized to zero, asymptotically approaches a quasi steady-state due to the balance between mean gradient production and scalar dissipation. We assume that the g-field has reached a statistically stationary state after 30 eddy turnover times, and thus use the remaining 30 eddy turnover times to compute statistical averages of the single-point and spectral quantities. Running the simulations for such long times ensures that we obtain meaningful statistical measures of the mean scalar quantities of interest. Spherically averaged scalar autocorrelation, dissipation, and scalar-velocity cross correlation spectra are determined from sums over shells by the following formulae:

$$E_g(k) = \sum_{\phi=0}^{\phi=2\pi} \sum_{\mu=-1}^{\mu=1} [g(\boldsymbol{k})g^*(\boldsymbol{k})]\Big|_{k_i-\Delta k/2\leqslant|\boldsymbol{k}|\leqslant k_i+\Delta k/2} \tag{17}$$

$$k^2 E_g(k) = \sum_{\phi=0}^{\phi=2\pi} \sum_{\mu=-1}^{\mu=1} \boldsymbol{k}\cdot\boldsymbol{k}[g(\boldsymbol{k})g^*(\boldsymbol{k})]\Big|_{k_i-\Delta k/2\leqslant|\boldsymbol{k}|\leqslant k_i+\Delta k/2} \tag{18}$$

$$E_{u_3 g}(k) = \sum_{\phi=0}^{\phi=2\pi} \sum_{\mu=-1}^{\mu=1} \frac{1}{2}[u_3(\boldsymbol{k})g^*(\boldsymbol{k}) + u_3^*(\boldsymbol{k})g(\boldsymbol{k})]\Big|_{k_i-\Delta k/2\leqslant|\boldsymbol{k}|\leqslant k_i+\Delta k/2} . \tag{19}$$

The stationary energy spectra from the DNS and model are presented in figure 1. Both energy spectra have a Reynolds number based on the integral scale of 223, although the values for the rms velocity and integral length scale are slightly different (see table 1). The disparity between the two spectra at small wavenumbers can be attributed to differences in the forcing schemes. In the DNS, the first two modes are required to produce the classical $k^{-5/3}$ scaling. The deterministic forcing used in the model only ensures that the energy added to the first two modes at each time step is identical to that lost through viscous dissipation. No inertial range scaling is imposed on the modelled spectrum, which via the form of the eddy damping terms (Pouquet *et al* 1975), produces the classic Kolmogorov scaling over a limited range of wavenumbers. The much closer agreement at higher wavenumbers

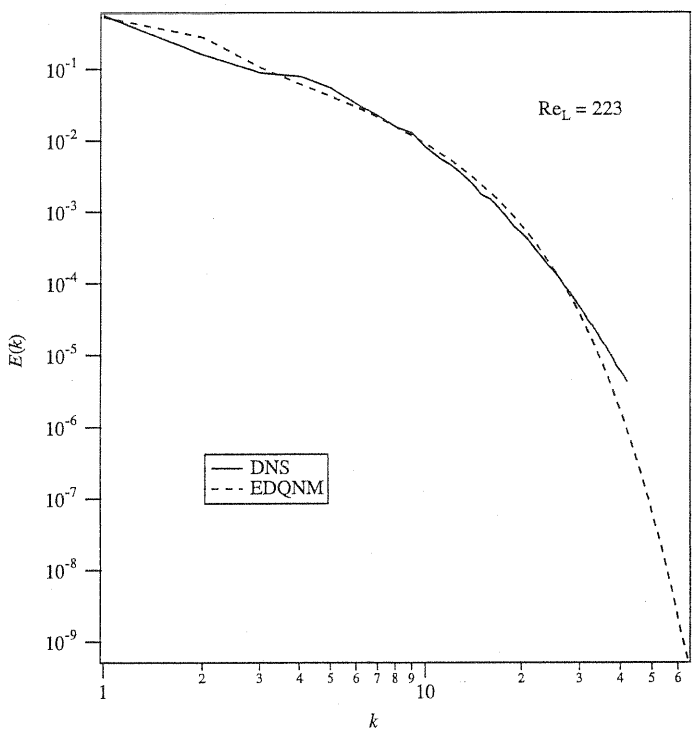

Figure 1. Steady-state energy spectrum for DNS and the model at $Re_L = 223$. Relevant single-point statistics corresponding to these spectra can be found in table 1.

Table 1. Comparison of velocity field parameters (in arbitrary units) for DNS and the EDQNM model. DNS results are obtained from time averages over the final 30 eddy turnover times of the simulation.

Parameter	Definition	DNS	Model
u'	Turbulence intensity	0.84	0.87
ϵ	Dissipation rate	0.19	0.19
ν	Kinematic viscosity	0.006	0.006
L	Integral length scale	1.59	1.54
λ	Taylor microscale	0.58	0.60
η	Kolmogorov length scale	0.033	0.033
T_e	Eddy turnover time	1.9	1.8
$s_{L0}L_m$	Scalar diffusivity	0.21	0.21
Re_L	Reynolds number (integral scale)	223	223
Re_λ	Reynolds number (microscale)	81	86

confirms that the behaviour of the small scales of turbulence are essentially uncoupled from the large eddies in the flow field (which are directly affected by the low wavenumber forcing).

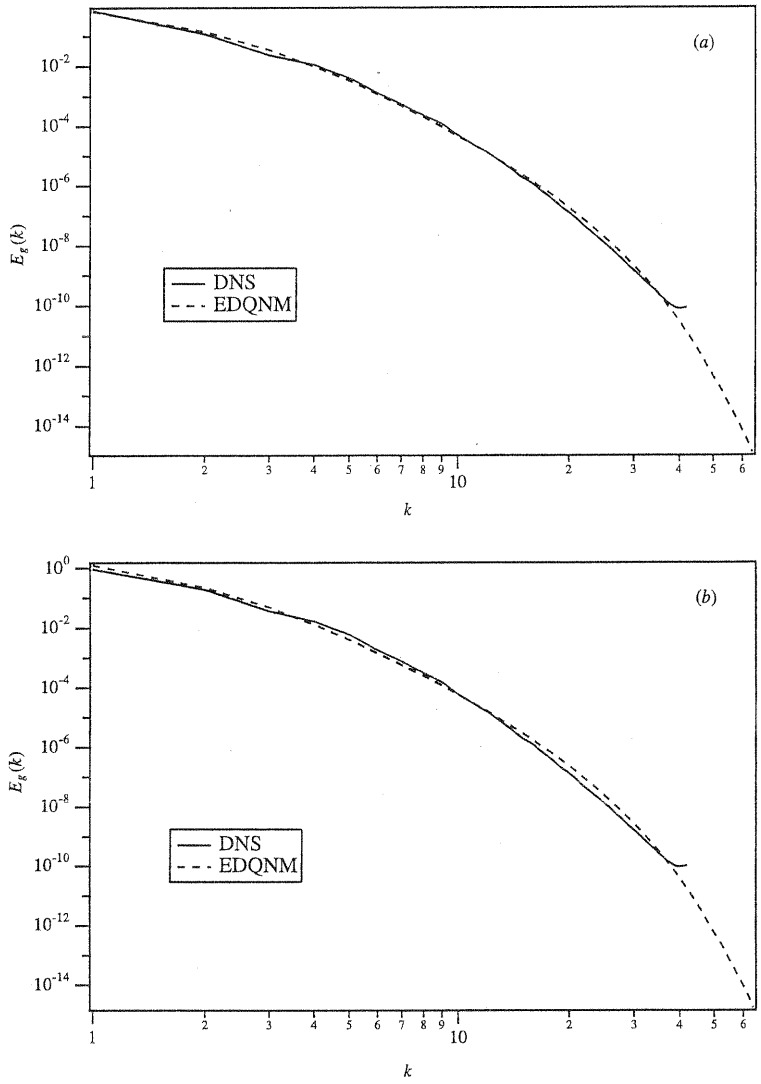

Figure 2. (*a*) Steady-state scalar autocorrelation spectrum for $u'/s_{L0} = 1$. (*b*) Same as (*a*), except that $u'/s_{L0} = 3$.

Figure 2 shows the autocorrelation spectrum at $u'/s_{L0} = 1$ and 3, respectively. The agreement is excellent over all wavenumbers, for both values of the dimensionless turbulence intensity. Note that the 'bump' in the energy spectrum arising from the forcing does not affect the smoothness of the scalar spectra or introduce any contamination into the scalar transfer process. The scalar rms values for the model and simulation (along with other single-point quantities) are given in table 2. Figure 3 contains the scalar dissipation spectrum

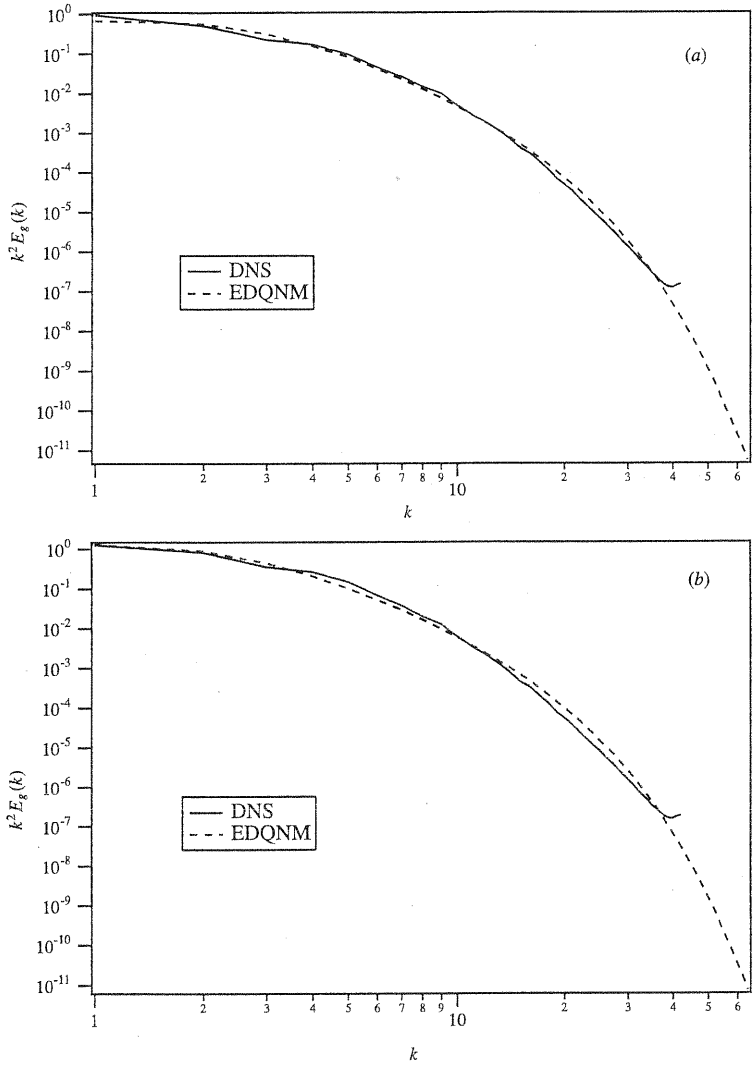

Figure 3. (*a*) Steady-state scalar dissipation spectrum for $u'/s_{L0} = 1$. (*b*) Same as (*a*), except that $u'/s_{L0} = 3$.

at $u'/s_{L0} = 1$ and 3. Not surprisingly, these spectra also compare favourably over the entire range of wavenumbers. The ratio of the turbulent to laminar flame speed is shown in equation (15). From table 2, we observe that there is good agreement between the flame speeds at both values of u'/s_{L0}. Figure 4 shows the scalar-velocity cross correlation spectrum at the two values of u'/s_{L0}. From these plots, as well as the others presented thus far, it appears that the model does quite well at predicting the steady-state behaviour of the flame front.

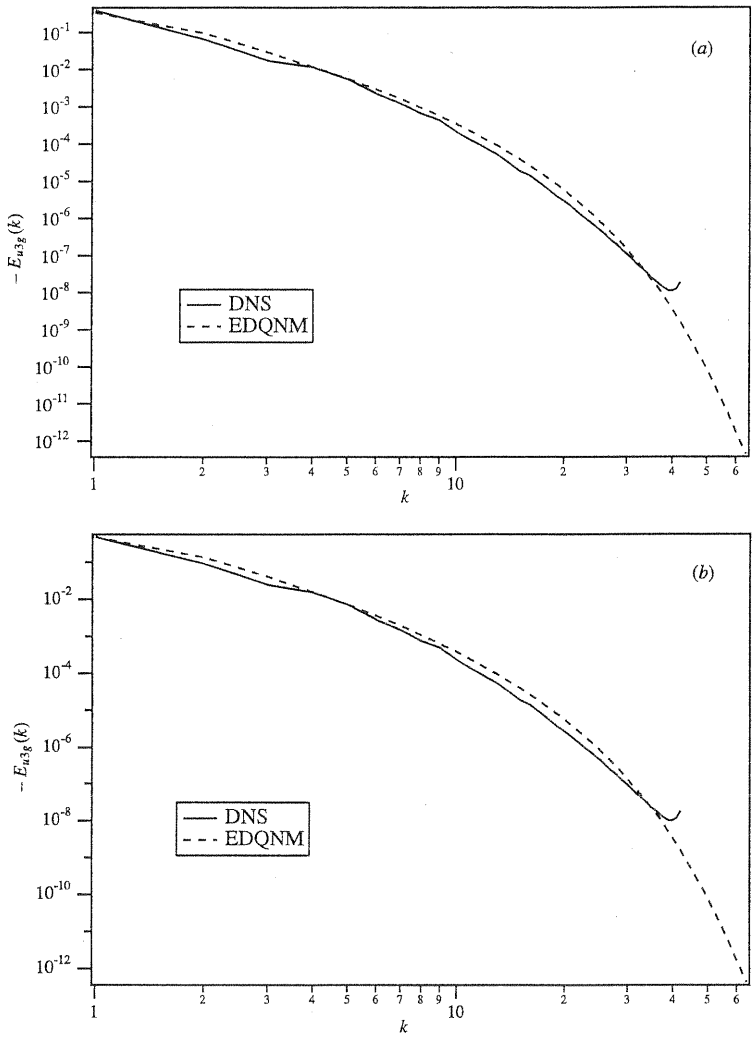

Figure 4. (*a*) Steady-state scalar-velocity cross correlation spectrum for $u'/s_{L0} = 1$. (*b*) Same as (*a*), except that $u'/s_{L0} = 3$.

At the start of each simulation, the flame front is perfectly flat; thus, the turbulent and laminar flame speeds are identical. However, turbulence very quickly wrinkles the flame front, generating surface area and causing the turbulent flame speed to increase. We can use the EDQNM model to track the time evolution of the flame speed ratio (s_T/s_{L0}) for the two values of u'/s_{L0}. These results are displayed in figure 5. It is interesting to note that the DNS and model are in almost perfect agreement for about the first eddy turnover time. The model then starts to asymptote to its steady-state value, while the DNS

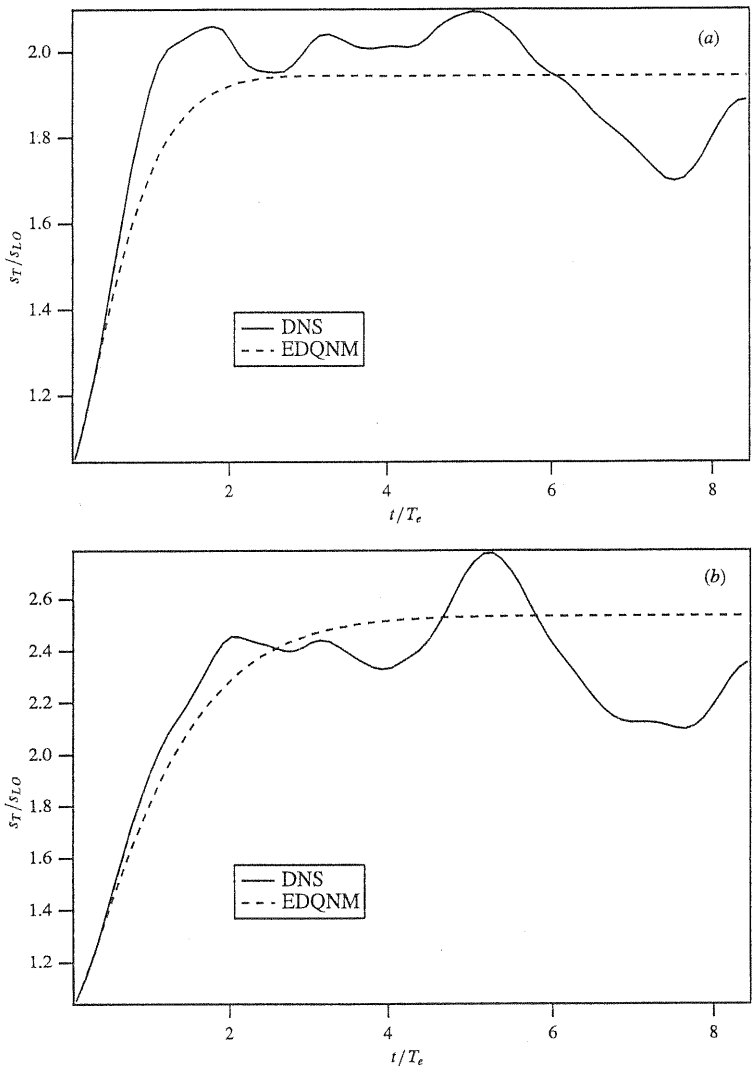

Figure 5. (*a*) Turbulent to laminar flame speed ratio as a function of dimensionless time for $u'/s_{L0} = 1$. (*b*) Same as (*a*), except that $u'/s_{L0} = 3$.

exhibits large fluctuations about its mean value. The fluctuations in the DNS are associated with the specific realization that is computed. In principle, these fluctuations could be eliminated (or at least reduced) by averaging over an ensemble of realizations, however, the computational cost required is prohibitive. Nevertheless, the quantitative agreement early on and the apparent agreement beyond the first few eddy turnover times is very encouraging.

Table 2. Comparison of single-point quantities resulting from DNS and EDQNM model predictions.

Quantity	Definition	u'/s_{L0}	DNS	Model
$g_{\rm rms}$	$\sqrt{\int_0^{k_{\max}} E_g(k)\,\mathrm{d}k}$	1	0.92	0.92
		3	1.08	1.25
s_T/s_L	See equation (15)	1	2.01	1.94
		3	2.48	2.53
$-\overline{u_3' g'}$	$-\int_0^{k_{\max}} E_{u_3 g}(k)\,\mathrm{d}k$	1	0.50	0.49
		3	0.62	0.67

4. Experimental method

A schematic of the experimental system is shown in figure 6. The experiment has been described in detail elsewhere (Ghenaï 1995, Ghenaï *et al* 1996), hence here only a brief summary of the experimental set-up will be given. The flame configuration used in this study is an open conical turbulent premixed flame. Premixed methane–air flames are stabilized by an annular pilot at the rim of the 25 mm inner diameter burner. The equivalence ratio is fixed throughout at the value $\Phi = 0.75$. Turbulence is produced by passing the reactant feed through a series of perforated plates 50 mm upstream of the burner exit. The turbulence parameters are then varied by changing the bulk velocity of the reactants ($U = 2$ and 5 m s^{-1}), and by varying the size of the holes in the perforated plate ($d_h = 2.5$ and 3.5 mm). The turbulence characteristics are measured, in the absence of combustion, using laser Doppler anemometry (see table 3).

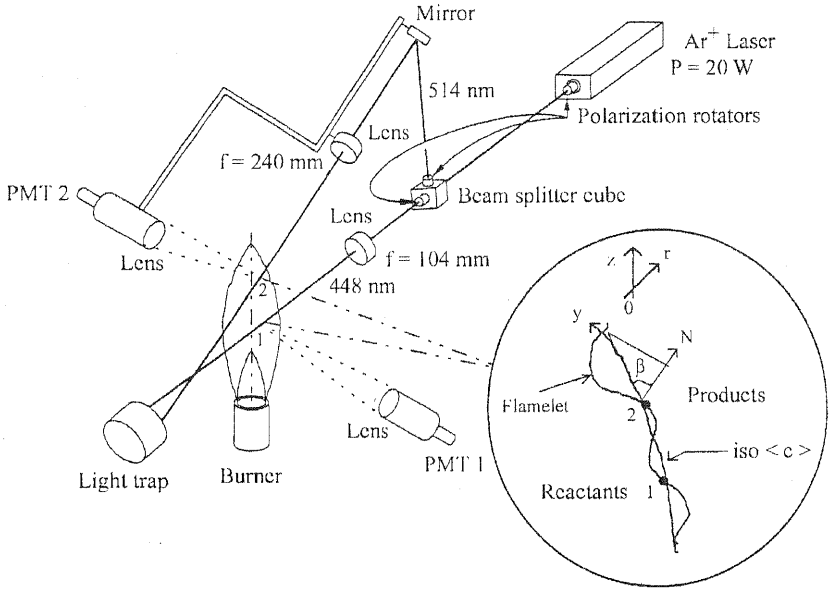

Figure 6. Schematic of the experimental apparatus.

Table 3. Experimentally measured turbulence and combustion parameters. U is the mean velocity measured at the burner exit, u' is the rms fluctuating velocity (axial direction), L is the integral length scale, s_{L0} is the unperturbed laminar flame speed, and d is the flame thickness. Variables to the right of the double line are dimensionless (note Da is the Damköhler number). The equivalence ratio was fixed at 0.75.

Case	U (m s^{-1})	u' (m s^{-1})	L (mm)	s_{L0} (m s^{-1})	d (mm)	u'/s_{L0}	Re_L	d/L	Da
(a)	2	0.11	3.1	0.27	0.24	0.42	22	0.077	34
(b)	5	0.275	3.1	0.27	0.24	1.02	55	0.077	13
(c)	5	0.50	4.7	0.27	0.24	1.85	151	0.051	11

The flames are analysed using laser-induced Rayleigh scattering (see figure 6). The experimental set-up allows for two-point density measurements along the longitudinal and radial directions. A 20 W Spectra Physics cw argon-ion laser is used as the light source. A beamsplitter separates the blue (488 nm) and green (514 nm) lines. The blue beam crosses the flame brush in a direction normal to the burner axis, as shown in figure 6. The green beam exits the beamsplitter parallel to the burner axis, but is then reflected into the flame at an angle controlled by the location of the mirror (see figure 6). Polarization rotators are then used to recover the correct polarization angles for maximum Rayleigh scattering efficiency. The two beams are focused down to a diameter of approximately 150 μm. The scattered light is collected by two Nikkor lenses ($f/d = 1.4$) with interference filters, and focused onto identical photomultipliers (Hamamatsu R647-04). The probe volume length for both PMTs is fixed at 150 μm wide; thus, the two measurement volumes correspond to cylinders of equal length with base diameters of 150 μm, which is of the order of the Zeldovich thickness of a stoichiometric methane/air flame.

Two-point Rayleigh scattering measurements require an accurate displacement system. In this set-up, the fixed optical probe volume is the one formed by the blue beam. Its position within the flame brush is adjusted by moving the burner, with a precision of 500 μm axially and 50 μm radially. The second optical probe volume, formed by the green beam, is displaced in the radial direction by moving the beamsplitter, mirror, and the PMT together. For the vertical displacement, only the mirror and the second PMT are moved axially. The precision of the displacement in either direction is estimated to be 10 μm.

The combination of both displacements allows two-point measurements to be obtained along a constant mean density (or constant mean progress variable) contour. This is the experimental analogue of the two-point spectra discussed earlier. The analogy is not perfect, however, and so a theoretical relationship between the experimental two-point correlation and the scalar spectrum computed by the model is required to make meaningful comparisons.

5. Transition from model to experiment

The description of flame propagation provided by the model and the numerical simulations differ in a fundamental way from the flame surface observed in a real experiment. The model and simulations describe the dynamics of an ensemble of flame surfaces, each represented by a different value of the field variable $G(x, t)$, whereas an experiment can only observe a single flame surface at a given instant. Consequently, the variables in the model and simulation vary *continuously*, whereas the signal from an experiment varies (nearly) *discontinuously* at the flame interface. The discontinuous signal measured in a premixed flame experiment is sometimes referred to as a 'telegraph signal' (Cheng *et al* 1989). Before we can make

comparisons with the experiments, we must correct for this difference.

In this section, we derive an approximate mathematical relationship between the spectrum obtained from the ensemble of flames, as is computed in the model, and the spectrum that describes a single flame. The result, although approximate, allows for a more meaningful comparison between experimental measurements made in the laboratory and the EDQNM model.

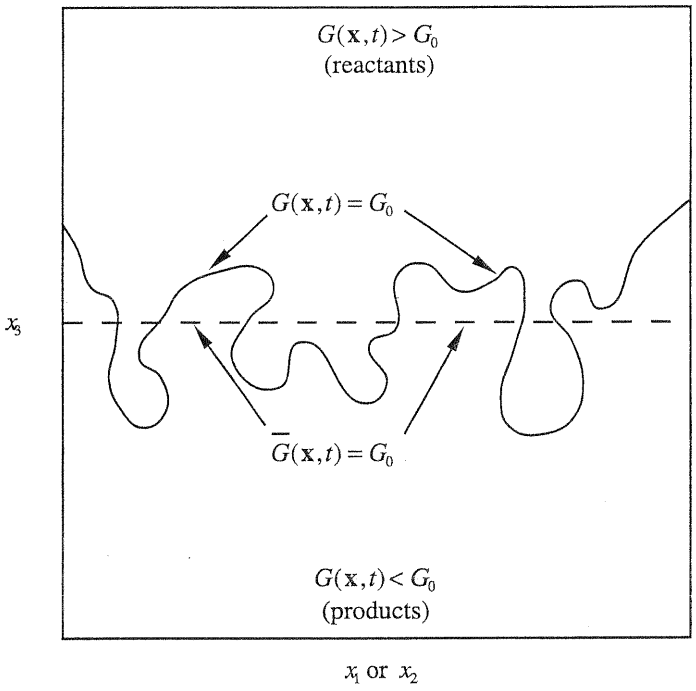

Figure 7. Two-dimensional sketch of a flame isocontour. Also shown is the line cutting through the midpoint of the flame brush, over which the 'telegraph signal' is measured. This signal will consist of a set of ones and zeros, depending on whether the reactant or product side of the flame is being sampled.

The conversion from model to experiment can be accomplished by considering only a *single* surface in the model corresponding to $G(\boldsymbol{x}, t) = G_0$, for example. Such a surface is shown schematically in figure 7, which depicts a two-dimensional slice through the propagating premixed flame defined by $G(\boldsymbol{x}, t) = G_0$. Using figure 7 as a departure point, we assume that we have a flame surface in three dimensions defined by $G(\boldsymbol{x}, t) = G_0$. To formally isolate a single surface from the ensemble, we define a variable $F(\boldsymbol{x}, t)$ such that

$$F(\boldsymbol{x}, t) \equiv H[G(\boldsymbol{x}, t) - G_0] = \begin{cases} 1 & \text{if} \quad G(\boldsymbol{x}, t) \geqslant G_0 \\ 0 & \text{if} \quad G(\boldsymbol{x}, t) < G_0 \end{cases} \tag{20}$$

where $H[\,]$ is the Heaviside (unit step) function. The function $F(\boldsymbol{x}, t)$ is defined to be unity everywhere within the reactants and zero everywhere within the products, thus mimicking the experimental flame. Recall that $G(\boldsymbol{x}, t)$ can be written in terms of $g(\boldsymbol{x}, t)$ as follows:

$$G(\boldsymbol{x}, t) = x_3 + g(\boldsymbol{x}, t) = x_3 + g'(\boldsymbol{x}, t) + \overline{g}(t) \tag{21}$$

where the turbulent flame speed is given by $s_T \equiv \mathrm{d}\overline{g}/\mathrm{d}t$. The experimental measurements that we wish to compare to our model are two-point correlations measured along the midpoint of the flame brush, i.e. $\overline{C} = 0.5$. In the model this corresponds to a planar cut along $x_3 + \overline{g}(t) = G_0$. Along that plane, the function $F(x, t)$ becomes a telegraph signal whose value depends on whether the flame surface is above ($F = 0$) or below ($F = 1$) the plane. The telegraph signal can be written mathematically as

$$F(x_1, x_2, G_0 - \overline{g}, t) = H[G(x_1, x_2, G_0 - \overline{g}, t) - G_0] = H[g'(x_1, x_2, G_0 - \overline{g}, t)]. \tag{22}$$

For notational purposes, it will be useful to define position vectors $\mathcal{X}$ and $\tilde{\mathcal{X}}$ as $\mathcal{X} \equiv (x_1, x_2, G_0 - \overline{g})$ and $\tilde{\mathcal{X}} \equiv (x_1 + r_1, x_2 + r_2, G_0 - \overline{g})$, respectively. Equation (22) now becomes

$$F(\mathcal{X}, t) = H[G(\mathcal{X}, t) - G_0] = H[g'(\mathcal{X}, t)]. \tag{23}$$

Experiments measure the correlation of the telegraph signal F at two points along the plane. Thus, we are interested in obtaining the two-point correlation of F in terms of the predicted spectrum of the g-field. A proper correlation should involve fluctuating, rather than total quantities. In order to derive a closed form expression for F', we need to consider the statistical distribution of g'. If we postulate that the probability density function (PDF) for g' is distributed symmetrically about 0, which physically suggests that positive and negative fluctuations are equally likely, then we arrive at the simple result that $\overline{F}(\mathcal{X}, t) = \overline{H[g'(\mathcal{X}, t)]} = \frac{1}{2}$. Thus, the fluctuating component is given by $F'(\mathcal{X}, t) = H[g'(\mathcal{X}, t)] - \frac{1}{2}$. The proper form of the correlation can now be expressed as

$$B_F(r) \equiv \overline{F'(\mathcal{X}, t)F'(\tilde{\mathcal{X}}, t)} = \overline{H[g'(\mathcal{X}, t)]H[g'(\tilde{\mathcal{X}}, t)]} - \tfrac{1}{4} \tag{24}$$

where $B_F(r)$ is the desired 'telegraph signal' correlation, $r \equiv |\mathcal{X} - \tilde{\mathcal{X}}|$, and we have used the relations $\overline{H[g'(\mathcal{X}, t)]} = \overline{H[g'(\tilde{\mathcal{X}}, t)]} = \frac{1}{2}$. Unfortunately, it is not sufficient to simply assume some symmetry property of g' to evaluate $B_F(r)$. That is, we must assume a *specific* joint distribution for $g'(\mathcal{X})$ and $g'(\tilde{\mathcal{X}})$, and recognize that our final result will be influenced by our choice of the PDF. At this stage, the assumption of a bivariate normal PDF seems reasonable and has the added advantage of producing an analytical result.

The joint normal or Gaussian PDF expressed in terms of the random variables Z_1 and Z_2 (corresponding to $g'(\mathcal{X})$ and $g'(\tilde{\mathcal{X}})$, respectively) has the form

$$p(Z_1, Z_2) = \frac{\mathrm{e}^{-(Z_1^2 - 2\sigma_{12}Z_1Z_2 + Z_2^2)/[2\sigma^2(1-\sigma_{12}^2)]}}{2\pi\sigma^2\sqrt{1-\sigma_{12}^2}} \tag{25}$$

where $\overline{Z_1^2} = \overline{Z_2^2} = \sigma^2$, $\overline{Z_1Z_2} = \sigma_{12}\sigma^2$, and σ_{12} is the correlation coefficient ($-1 \leqslant \sigma_{12} \leqslant 1$). Letting $g'(\mathcal{X}) = Z_1$ and $g'(\tilde{\mathcal{X}}) = Z_2$ implies

$$\begin{aligned} \sigma^2 &= \overline{g'^2} \\ \sigma^2\sigma_{12}(r) &= \overline{g'(\mathcal{X})g'(\tilde{\mathcal{X}})}. \end{aligned} \tag{26}$$

These two PDF parameters (σ^2 and $\sigma_{12}(r)$) are directly related to $E_g(k)$, the scalar autocorrelation spectrum calculated in the EDQNM model. The equations connecting the autocorrelation spectrum to the parameters are

$$\begin{aligned} \sigma^2 &= \int_0^{k_{\max}} E_g(k)\,\mathrm{d}k \\ \sigma^2\sigma_{12}(r) &= \int_0^{k_{\max}} \frac{\sin(kr)}{kr} E_g(k)\,\mathrm{d}k. \end{aligned} \tag{27}$$

The expression for $\sigma_{12}(r)$ involves an inverse sine transform. This type of transform occurs as a result of spherically integrating an isotropic spectrum (Batchelor 1953). Also, the r dependence of the correlation is entirely embedded within the variable $\sigma_{12}(r)$.

Given an arbitrary function of two random variables, its mean is determined by integrating the product of the function and the PDF over the domain spanned by Z_1 and Z_2. Therefore, the expectation for $H[g'(\mathcal{X}, t)]H[g'(\tilde{\mathcal{X}}, t)]$ is given by

$$\begin{aligned}\overline{H[g'(\mathcal{X}, t)]H[g'(\tilde{\mathcal{X}}, t)]} &= \int_{-\infty}^{\infty}\int_{-\infty}^{\infty} H[Z_1]H[Z_2]p(Z_1, Z_2)\,\mathrm{d}Z_1\,\mathrm{d}Z_2 \\ &= \int_{0}^{\infty}\int_{0}^{\infty} p(Z_1, Z_2)\,\mathrm{d}Z_1\,\mathrm{d}Z_2. \end{aligned} \tag{28}$$

Due to the on/off nature of the Heaviside function, the domain of integration is restricted to the first quadrant of the Z_1–Z_2 plane (i.e. when both Heaviside functions take the value of unity). The integrand can be simplified by defining

$$\begin{aligned}\alpha &= 2\pi\sigma^2\sqrt{1-\sigma_{12}^2(r)} \\ \beta &= \sigma\sqrt{2(1-\sigma_{12}^2(r))} \\ \tilde{Z}_1 &= Z_1/\beta \\ \tilde{Z}_2 &= Z_2/\beta. \end{aligned} \tag{29}$$

The integration now takes the form

$$\int_0^{\infty}\int_0^{\infty} p(Z_1, Z_2)\,\mathrm{d}Z_1\,\mathrm{d}Z_2 = \frac{\beta^2}{\alpha}\int_0^{\infty}\int_0^{\infty} \mathrm{e}^{-\tilde{Z}_1^2-\tilde{Z}_2^2+2\sigma_{12}\tilde{Z}_1\tilde{Z}_2}\,\mathrm{d}\tilde{Z}_1\,\mathrm{d}\tilde{Z}_2. \tag{30}$$

By switching to polar coordinates, where $\tilde{Z}_1 = \tilde{r}\cos\theta$ and $\tilde{Z}_2 = \tilde{r}\sin\theta$, the $\tilde{r}$ integration can be performed analytically yielding

$$\frac{\beta^2}{\alpha}\int_0^{\pi/2}\int_0^{\infty} \mathrm{e}^{-\tilde{r}^2(1-\sigma_{12}(r)\sin 2\theta)}\tilde{r}\,\mathrm{d}\tilde{r}\,\mathrm{d}\theta = \frac{\beta^2}{2\alpha}\int_0^{\pi/2}\frac{m\,\mathrm{d}\theta}{1-\sigma_{12}(r)\sin 2\theta}. \tag{31}$$

Equation (31) can also be integrated analytically, producing the final desired result

$$\begin{aligned}B_F(r) &= \overline{H[g'(\mathcal{X}, t)]H[g'(\tilde{\mathcal{X}}, t)]} - \tfrac{1}{4} \\ &= \frac{1}{2\pi}\arctan\left[\frac{\sigma_{12}(r)}{\sqrt{1-\sigma_{12}^2(r)}}\right]. \end{aligned} \tag{32}$$

It is standard practice to normalize correlations by their value at $r = 0$. As $\sigma_{12}(0) = 1$, equation (32) yields the result that $B_F(0) = \frac{1}{4}$. Thus the final normalized form of the correlation is

$$\tilde{B}_F(r) \equiv \frac{B_F(r)}{B_F(0)} = \frac{2}{\pi}\arctan\left[\frac{\sigma_{12}(r)}{\sqrt{1-\sigma_{12}^2(r)}}\right]. \tag{33}$$

6. Comparison with experiment

The dimensionless parameter values associated with the three sets of experimental measurements to which we compare the EDQNM model are given in table 3. For the model, it is not sufficient to characterize the hydrodynamic field with only a Reynolds number, rather, an entire energy spectrum must be specified. Since the Pao energy spectrum previously has been shown to compare well with experimental data (Hinze 1975, McComb 1994), we have chosen this analytic spectrum as an input to the model. This spectrum consists of a classical $k^{-5/3}$ inertial range followed by exponential decay in the dissipation region. Figure 8 shows the three Pao energy spectra used in this study as well as the analytic equation for the Pao spectrum. Also, in an effort to obtain better resolution of the large scales of turbulence in the model, we have employed a logarithmic (Lesieur and Schertzer 1978), as opposed to a uniform, discretization with $k_m = e^{m\Delta k}$, $0 \leqslant m \leqslant 200$, and $\Delta k = 0.03$.

Figure 9 shows the model and experimental correlations for cases (a) and (b), respectively (the correlation from the EDQNM model is calculated from equation (33)). The marked disagreement in figure 9(*a*) can be attributed, in part, to the very low value of the Reynolds number. It is likely that the flame is mainly encountering well defined vortical structures, as opposed to the nearly Gaussian turbulence assumed by the model. As EDQNM is a spectral model with no phase information, it lacks the ability to describe the coherent part of the flow field. Also, several of the eddy damping constants for the model have been determined by appealing to conservation arguments in the limit of *infinite* rather than zero Reynolds number (Andre and Lesieur 1977). There is improved agreement for case (b) shown in figure 9(*b*).

Figure 10 shows the experimental and model physical space correlations for case (c) along with the uncorrected (broken curve) model correlation for the ensemble of flame surfaces (calculated by $\sigma_{12}(r)/\sigma^2$). Here we observe good agreement between $\tilde{B}_F(r)$ at small

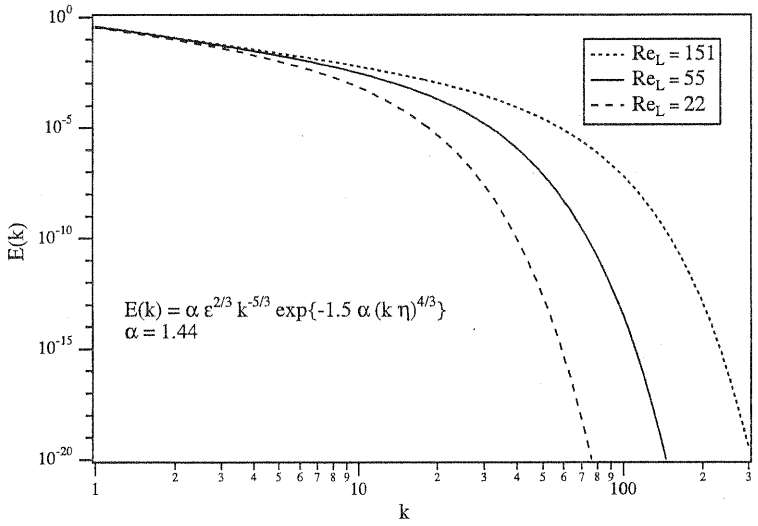

Figure 8. Dimensionless Pao energy spectra used for experimental data comparison. Note that η is the Kolmogorov scale defined as $(\nu^3/\epsilon)^{1/4}$, L is the integral length scale and u' is the rms fluctuating velocity.

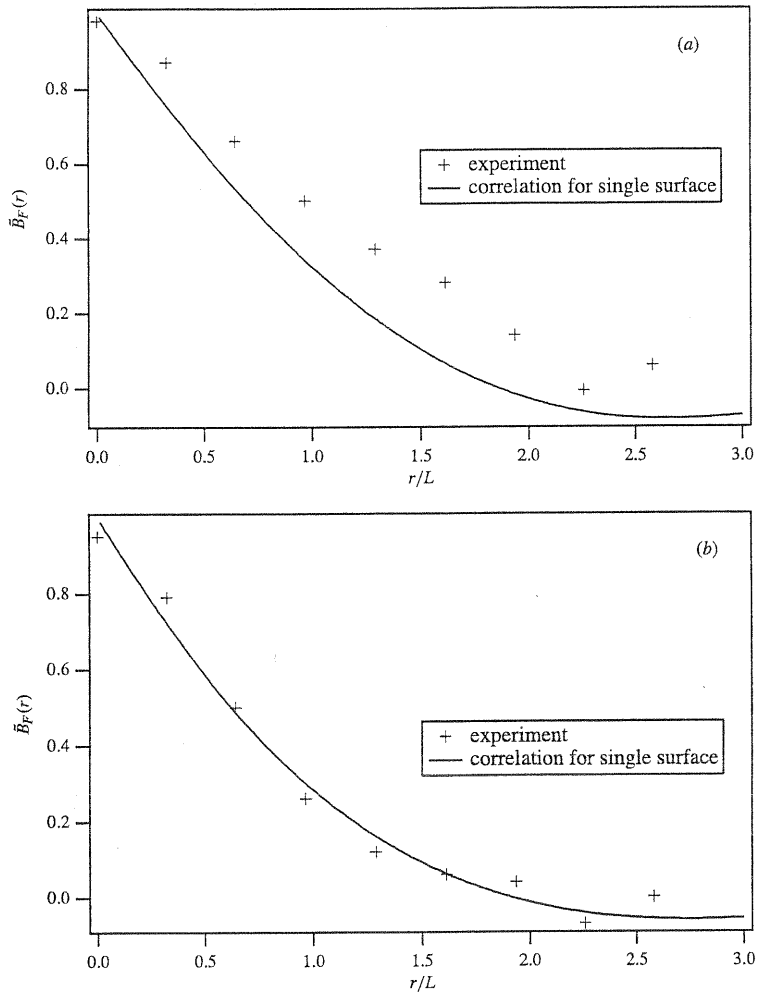

Figure 9. (*a*) Comparison of spatial correlation for case (a), $Re_L = 22$ and $u'/s_{L0} = 0.42$. (*b*) Comparison of spatial correlation for case (b), $Re_L = 55$ and $u'/s_{L0} = 1.02$.

and large values of dimensionless distance, with the majority of the error taking place at intermediate values of r/L. However, there is more pronounced scatter in the data measured at these conditions than was observed in the less turbulent ones. It is also important to note the difference between corrected (see equation (33)) and uncorrected curves. It appears as though in transitioning from an ensemble of surfaces to a single flame surface, that the correlation is depressed over most values of r/L, in apparent agreement with the experimental measurements. A possible explanation for this depression may be attributed to the smoothness of the g-field, in which highly correlated parts of the surface are relatively unaffected by small changes in the separation distance. In contrast, in an actual flame surface represented by F, a small change in separation may cause a cross-over from reactant to product or

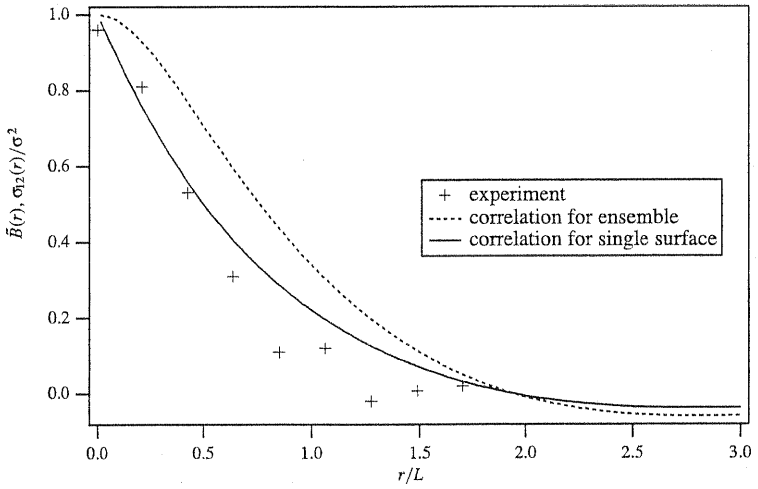

Figure 10. Comparison of spatial correlation for case (c), $Re_L = 151$ and $u'/s_{L0} = 1.85$ where we also include the ensemble correlation obtained by directly transforming $E_g(k)$.

vice versa. Since only cases in which both points of the correlation are in the reactant mixture contribute (as a result of the Heaviside function), it is reasonable that the ensemble correlation will be larger than the single-surface correlation. This figure supports the hypothesis that ensemble and single-surface data are not identical, and that a fair comparison can only be made between the corrected single-surface correlation and the experimental two-point measurements.

Another possible source of error in the EDQNM model has to do with neglecting thermo-diffusive and hydrodynamic effects (Dandekar and Collins 1995). Since the experiment uses a lean methane–air flame with equivalence ratio of 0.75, the Lewis number is greater than unity. Lewis numbers greater than unity are stabilizing, which will tend to shift the model correlation curves to the right (for fixed values of Re_L, u'/s_{L0}, and d/L). The hydrodynamic effect, however, is always destabilizing, and will tend to offset the stabilizing effect of the Lewis number when it is above unity. As noted earlier, hydrodynamic instabilities cannot be incorporated into the present Markovianization step in the EDQNM procedure; we therefore have opted to neglect both effects.

7. Conclusions

In this study, we have presented a new spectral flamelet model derived from the Kuramoto–Sivashinsky equation for the flame surface and the EDQNM turbulence theory. The main goal of the study was to validate the closure assumptions that were used to derive the spectral transport equations as well as to make comparisons of the model predictions with experimental measurements. To accomplish the first goal, we presented detailed comparisons of the model with DNS. These comparisons test the EDQNM closure approximations for the triple correlations, including new ones that arise from the propagation term. In the second part of the study, we showed comparisons of the model with two-point measurements in a lean methane–air flame, enabling us to assess how well the Kuramoto–Sivashinsky equation represents a real turbulent premixed flame.

Direct numerical simulations of the Kuramoto–Sivashinsky equation were performed on a grid containing 128^3 nodes (corresponding to a Reynolds number based on the integral length scale of 223) at two different values of u'/s_{L0}. Predictions of the scalar autocorrelation, dissipation and scalar–velocity spectra were in excellent agreement with the DNS. In addition, good agreement was observed for all of the single-point quantities, both at steady state and during the transient period before the flame had equilibrated with the turbulence.

Before comparing the model predictions with experimental measurements, we had to derive a relationship between the autocorrelation spectrum obtained from the field equation, representing a spectral correlation among an ensemble of flame surfaces, and the experimental correlation measured from a single flame surface (at an instant). This relationship requires information on the joint probability of the scalar variables at two points, which is not provided by the model; here we assumed the two-point distribution to be joint Gaussian. An important advantage of choosing the joint Gaussian distribution is that the resulting expression for converting between the two representations is analytic. Of course, the accuracy of the expression depends on the reliability of the assumed shape. An alternative approach would be to use experimental measurements of the two-point distribution to numerically convert one spectrum into the other; however, such an approach would be cumbersome to use, in general.

An experimental set-up for generating a lean premixed methane–air flame was then presented. Reasonably good agreement between the model and experiment was observed for the three considered cases: (a) $Re_L = 22$, $u'/s_{L0} = 0.42$, $d/L = 0.077$, (b) $Re_L = 55$, $u'/s_{L0} = 1.02$, $d/L = 0.077$, (c) $Re_L = 151$, $u'/s_{L0} = 1.85$, $d/L = 0.051$, with most of the error taking place at the lowest Reynolds number. It was also shown that there is a significant difference between the model correlations representing an ensemble of flame surfaces and those describing a single flame surface.

Although experimental measurements along the midpoint of the flame brush result in physical space correlations, it is often instructive to compute the Fourier transform or spectrum of the autocorrelation. As the correlation is computed in a *plane* transverse to the direction of nominal flame propagation, a two-dimensional Fourier transform is required. In two dimensions, the transform kernel involves a zeroth-order Bessel function of the first kind, $J_0(kr)$ (Kraichnan 1970), in contrast to the trigonometric kernel that shows up in three dimensions. This result can be easily derived from the definition of the two-dimensional forward Fourier transform, yielding

$$E_g^*(k) = \int_0^{r_{\max}} kr J_0(kr) \tilde{B}_F(r)\, \mathrm{d}r$$

where $E_g^*(k)$ represents the two-dimensional autocorrelation spectrum and has the property that its integral over all length scales in Fourier space is unity. A future study will focus on making comparisons between the autocorrelation spectrum predicted by the EDQNM model and experimental measurements.

Acknowledgments

All numerical simulations were performed on the massively parallel CM-5 at Los Alamos National Laboratory. Financial support for this study was provided in part by Dow Chemical and Arco Chemical (in separate awards to LRC). The experimental work performed at the LCSR (Laboratoire de Combustion et Sysèmes Réactifs) was supported by the CNRS (Centre National de la Recherche Scientifique) agency in France. The international collaboration between IG and LRC is also supported by the joint NSF/CNRS grant INT-9815832.

References

Aldredge R C 1992 The propagation of wrinkled premixed flames in spatially periodic shear flow *Combust. Flame* **90** 121

Andre J C and Lesieur M 1977 Influence of helicity on the evolution of isotropic turbulence at high Reynolds number *J. Fluid Mech.* **81** 187

Ashurst W T and Sivashinsky G I 1991 On flame propagation through periodic flow fields *Combust. Sci. Technol.* **80** 159

Ashurst W T, Sivashinsky G I and Yakhot V 1988 Flame front propagation in nonsteady hydrodynamic fields *Combust. Sci. Technol.* **62** 273

Batchelor G K 1953 *The Theory of Homogeneous Turbulence* (Cambridge: Cambridge University Press)

Cambon C, Jeandel D and Mathieu J 1981 Spectral modelling of homogeneous non-isotropic turbulence *J. Fluid Mech.* **104** 247

Canuto C, Hussaini M Y, Quarteroni A and Zang T A 1988 *Spectral Methods in Fluid Dynamics* (New York: Springer)

Cheng R K, Sheperd I G and Gökalp I 1989 A comparison of the velocity and scalar spectra in premixed turbulent flames *Combust. Flame* **78** 205–21

Clavin P and Joulin G 1997 High-frequency response of premixed flames to weak stretch and curvature: a variable-density analysis *Combust. Theory Modelling* **1** 429–46

Clavin P and Williams F A 1982 Effects of molecular diffusion and of thermal expansion on the structure and dynamics of premixed flames in turbulent flows of large scale and low intensity *J. Fluid Mech.* **116** 251

Collins L R 1995a Fractal geometry of a numerically simulated flame surface *IEC Research* **34** 2588

——1995b Spectral analysis of a simulated premixed flame surface in two dimensions *Comput. Fluids* **24** 663

Collins L R and Ulitsky M 1996 Spectral model of premixed flame propagation *Proc. Combust. Inst.* **26** 315

Damköhler G 1940 The effect of turbulence on the flame velocity in gas mixtures *Z. Electrochem.* **46** 601 (Engl. transl. 1947 *NACA TM* **1112**)

Dandekar A and Collins L R 1995 Effect of non-unity lewis number on premixed flame propagation through isotropic turbulence *Combust. Flame* **101** 428–40

Denet B 1998 Are small scales of turbulence able to wrinkle a premixed flame at large scale? *Combust. Theory Modelling* **2** 167

Eswaran V and Pope S B 1988 An examination of forcing in direct numerical simulations of turbulence *Comput. Fluids* **16** 257

Ghenaï C 1995 Etude de la structure et de la dynamique spatio-temporelle des fronts de flamme instantanés en combustion prémélangée *PhD Thesis* L'universite d'Orleans

Ghenaï C, Chauveau C and Gökalp I 1996 Spatial and temporal dynamics of flamelets in turbulent premixed flames *Proc. Combust. Inst.* **26** 331–7

Glassman I 1987 *Combustion* (New York: Academic)

Gouldin F C 1987 An application of fractals to modeling premixed turbulent flames *Combust. Flame* **68** 249

Herr S, Wang L-P and Collins L R 1996 EDQNM model of a passive scalar with a uniform mean gradient *Phys. Fluids* **8** 1588–608

Herring J R 1974 Approach of axisymmetric turbulence to isotropy *Phys. Fluids* **17** 859

Herring J R, Schertzer D, Lesieur M, Newman G R, Chollet J P and Larcheveque M 1982 A comparitive assessment of spectral closures as applied to passive scalar diffusion *J. Fluid Mech.* **124** 411

Hinze J O 1975 *Turbulence* (New York: McGraw-Hill)

Huang Z, Bechtold J K and Matalon M 1998 Weakly stretched premixed flames in oscillation flows *Combust. Theory Modelling* **2** 115–33

Joulin G 1994 On the response of premixed flames to time-dependent stretch and curvature *Combust. Sci. Technol.* **97** 219–29

Kerstein A R 1988 Fractal dimension of turbulent premixed flames *Combust. Sci. Technol.* **60** 391

Kerstein A R, Ashurst W T and Williams F A 1988 Field equation for interface propagation in an unsteady homogeneous flow field *Phys. Rev.* A **37** 2728

Kraichnan R H 1970 Diffusion by a random velocity field *Phys. Fluids* **13** 22–31

Lee T-W, North G L and Santavicca D A 1993 Surface properties of turbulent premixed propane/air flames at various lewis numbers *Combust. Flame* **93** 445

Leith C E 1971 Atmospheric predictability in two-dimensional turbulence *J. Atmos. Sci.* **28** 145

Lesieur M 1987 *Turbulence in Fluids, Stochastic and Numerical Modeling* (Boston MA: Nijhoff)

Lesieur M, Montmory C and Chollet J-P 1987 The decay of kinetic energy and temperature variance in three-dimensional isotropic turbulence *Phys. Fluids* **30** 1278

Lesieur M and Schertzer D 1978 Amortissement auto similaire d'une turbulence a grand nombre de Reynolds *J.*

Mechanique **17** 609
Mantzaras J, Felton P G and Bracco F V 1989 Fractals and turbulent premixed engine flames *Combust. Flame* **77** 215
McComb W D 1994 *The Physics of Fluid Turbulence* (Oxford: Clarendon)
Nakauchi N 1984 An application of the modified zero-fourth-cumulant approximation to homogeneous axisymmetric turbulance *J. Phys. Soc. Japan* **53** 1682
North G I and Santavicca D A 1990 The fractal nature of premixed turbulent flames *Combust. Sci Technol.* **72** 215
Orszag S A 1970 Analytical theories of turbulence *J. Fluid Mech.* **41** 363
Osher S and Sethian J A 1988 Fronts propagating with curvature dependent speed: algorithms based on Hamilton–Jacobi formulations *J. Comput. Phys.* **79** 12
Peters N 1988 Laminar flamelet concepts in turbulent combustion *Proc. Combust. Inst.* **22** 1231
——1992 A spectral closure for premixed turbulent combustion in the flamelet regime *J. Fluid Mech.* **242** 611
Pouquet A, Lesieur M, Andre J C and Basdevant C 1975 Evolution of high Reynolds number two-dimensional turbulence *J. Fluid Mech.* **72** 305
Sivashinsky G I 1977 Non-linear analysis of hydrodynamic instability in laminar flames—I. Derivation of basic equations *Acta Astronautica* **4** 1177
——1979 On self-turbulization of a laminar flame *Acta Astronautica* **6** 569
——1983 Instabilities, pattern formation and turbulence in flames *Ann. Rev. Fluid Mech.* **15** 179
——1988 Cascade renormalization theory of turbulent flame speed *Combust. Sci. Technol.* **62** 77
Ulitsky M and Collins L R 1997a Application of the eddy damped quasi-normal markovian spectral transport theory to premixed turbulent flame propagation *Phys. Fluids* **9** 3410–30
——1997b Relative importance of coherent structures vs background turbulence in the propagation of a premixed flame *Combust. Flame* **111** 257–75
Wang L-P, Chen S and Brasseur J G 1999 Examination of hypotheses in Kolmogorov refined turbulence theory through high-resolution simulations, part 2. Passive scalar field *J. Fluid Mech.* **400** 163–97
Wang L P, Chen S, Brasseur J G and Wyngaard J C 1996 Examination of hypotheses in Kolmogorov refined turbulence theory through high-resolution simulations I. Velocity field *J. Fluid Mech.* **309** 113
Yakhot V 1988 Propagation velocity of premixed turbulent flames *Combust. Sci. Technol.* **60** 191
Zhu J and Ronney P D 1994 Simulation of front propagation at large non-dimensional flow disturbance intensities *Combust. Sci. Technol.* **100** 183